Heat and Technology
Vol. 32, n. 1-2, 2014

NUMERICAL SIMULATION OF TWO-PHASE FLOW MODELING OF SOLID PROPELLANT COMBUSTION

Mahmoud Rashad*, XaioBing Zhang*

*School of Energy and Power Engineering, Nanjing University of Science and Technology
mahmodmosa2004@yahoo.com; zhangxb680504@163.com

ABSTRACT

Up to date munitions developments are the leading stimulus to go through realistic investigations for the complex phenomenon occurs during interior ballistic cycle. Fast and accurate model is required to assure firing safety and performance of the guided projectile. In this paper, based on two-fluid model approach; a reactive two-phase flow model for the combustion process of solid granular propellant is developed. The model includes the governing equations of mass, momentum and energy for both phases as well as the constitutive laws. An accurate second order numerical technique is utilized to solve the system of equations. Sod shock tube problem is utilized to test the ability of the used numerical algorithm in solving the initial boundary value problem for the system of equations with shock wave behavior. The results of the numerical method are compared to the exact solution of a test problem for verification. The moving control volume conservation method is used to handle the moving boundary as well as a self-adapting grid algorithm is used to expand the computational domain to deal with the projectile motion. Simulation results are validated with an experimental data for validation. The interior ballistics performance is closely predicted using the developed model and the numerical code.

1. INTRODUCTION

Events inside gun chamber possess a transient behavior coupled with complex reactions under high pressure and temperature conditions. At the same time guided munitions must survive against rigorous loads during gun firing and deliver its intended utility at the target. Early interior ballistics models, which appeared in abundance as computer codes, are of the zero-dimensional variety [1]. These models exemplify such assumptions as uniform and instantaneous ignition of the entire propellant charge, with combustion taking place in a smoothly varying, well-stirred mixture [2-5]. Although lumped parameters models have the advantages of simplicity and being facilitate parametric analysis and optimizations with minimal computer resources, it cannot address the physical hydrodynamics of the problem as manifested in ignition-induced pressure waves [6]. Continually incidence of catastrophic failures in conventional guns was ultimately traced to ignition and combustion instability problems [7-9]. Two-phase flow problems are solved through two approaches; the Eulerian-Eulerian approach and Eulerian-Lagrangian approach. Models based on Eulerian-Eulerian approach [10-14], also called two-fluid models, consider the gas and solid phase as two continuum flow phases, with each having its mass, momentum, and energy equations, respectively. These models have the advantages in such cases where the density of solid particles possesses high values and the solid phase volume fraction could be an effective parameter. So, such models are appropriate and popular in most interior ballistic numerical simulations. On the other hand, models based on Eulerian-Lagrangian approach treat the gas phase as continuum, which modeled by the local averaged equations at the macroscopic scale, while the solid phase is treated as an individual particle which can be traced in space and time [15-20]. This approach has advantages that it can handle poly-dispersed particle size distributions as well as predicting two-phase flows including particles that have large accelerations. But such models are complex and need a huge computer resources as well as long time during run compared to Eulerian-Eulerian models.

In this work, a mathematical model based on Eulerian-Eulerian approach for a gas-solid flow of solid granular propellant and its products of combustion inside the gun barrel in large caliber naval gun guided projectile system is developed. The model includes the balance equations of mass, momentum and energy for both phases as well as necessary constitutive laws. MacCormack's technique is utilized to solve the hyperbolic system of equations [21]. G.A. Sod shock tube test is utilized to verify the ability of MacCormack's algorithm in solving the initial boundary value problem for the system of equations with shock wave behavior [22]. The moving control volume conservation (MCVC) method is established to handle the moving boundary as well as a self-adapting method was used to expand the computational domain in order to follow the movement of the projectile down the gun bore [23-25]. Figure 1 illustrates schematically the configuration of a typical granular propellant charge. The predicted numerical results are validated with experimental data.

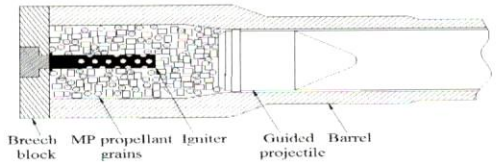

Fig.1-Schematic illustration of propellant charge in large caliber naval guided-projectile gun system.

2. THEORETICAL MODEL

The physical events, criterion of ignition, flame spreading and combustion of propellant grains inside the gun chamber can be referred to [20]. Based on charge configuration shown in Fig.1a, two-phase flow mathematical model is established using an Eulerian–Eulerian approach that was described in the introduction section. The interaction processes between the solid and gas phase are added to single-phase conservation laws via source terms. The governing equations are constructed from the mass and momentum conservation laws for both phases and the energy conservation law for the gas phase. Since the model assumes propellant grains are incompressible, there is no energy equation for the solid phase. The equations of various phases are presented below as follows:

Mass conservation equation of the gas phase:

$$\frac{\partial(\varphi\rho_g A)}{\partial t}+\nabla\cdot(\varphi\rho_g u_g A)=\dot{m}_c A+\sum\dot{m}_{ign}A \tag{1}$$

Mass conservation equation of the solid phase:

$$\frac{\partial[(1-\varphi)\rho_p A]}{\partial t}+\nabla\cdot[(1-\varphi)\rho_p u_p A]=-\dot{m}_c A \tag{2}$$

Momentum conservation equation of gas phase:

$$\frac{\partial(\varphi\rho_g u_g A)}{\partial t}+\nabla\cdot(\varphi\rho_g u_g u_g A)= -f_s A+\dot{m}_c u_p A+\sum\dot{m}_{ign}u_{ign}A-(\varphi A)\nabla p \tag{3}$$

Momentum conservation equation of solid phase:

$$\frac{\partial[(1-\varphi)\rho_p u_p A]}{\partial t}+\nabla\cdot[(1-\varphi)\rho_p u_p u_p A]+ \nabla[(1-\varphi)R_p A]= f_s A-\dot{m}_c u_p A-(1-\varphi)A\nabla p \tag{4}$$

Energy conservation equation of the gas phase:

$$\frac{\partial[\varphi\rho_g A(e_g+u_g\cdot u_g/2)]}{\partial t}+\nabla\cdot[\varphi\rho_g u_g A(e_g+ p/\rho_g+u_g\cdot u_g/2)] =-Q_p A-f_s u_p A+\dot{m}_c A(e_p+ p/\rho_p+u_p\cdot u_p/2) +\sum\dot{m}_{ign}H_{ign}A-p\frac{\partial(A\varphi)}{\partial t} \tag{5}$$

In the previous equations, φ is the volume fraction of the gas phase, ρ_g, ρ_p are gas and solid density, u_g ,u_p are gas and solid velocity, P ,e_g are pressure and internal energy of the gas-phase, m_c is the rate of gas mass generation due to propellant combustion, m_{ign} is the mass flow rate of gas from the vent-holes on the igniter, H_{ign} is stagnation enthalpy of the gas flow from the vent-holes on the igniter, f_s, Q_p , R_p are interphase drag, interphase heat transfer and intergranular stress, respectively. The constitutive relations those needed to close the above governing equations and to express the interaction between the two phases such as interphase drag, intergranular stress, heat transfer and so on are necessary. For more details, we refer to [21, 22, 36 and 37].

3. NUMERICAL APPROACH

3.1 MacCormack 's technique

Equations (1-5) for the one dimensional two-phase reactive flow can be written in the form of conservation laws for simplifying the numerical solution as:

$$\frac{\partial U}{\partial t}+\frac{\partial E}{\partial x}=S \tag{6}$$

Where, U , E , S are the conserved variables, the flux vector and the source vector respectively.

The components of U are the conserved variables can be written as:

$$U=\begin{pmatrix}U_1\\U_2\\U_3\\U_4\\U_5\end{pmatrix}=\begin{pmatrix}\varphi\rho_g A\\(1-\varphi)\rho_p A\\\varphi\rho_g u_g A\\(1-\varphi)\rho_p u_p A\\\varphi\rho_g(e_g+u_g^2/2)A\end{pmatrix} \tag{7}$$

And the components of E are the flux functions:

$$E=\begin{pmatrix}E_1\\E_2\\E_3\\E_4\\E_5\end{pmatrix}=\begin{pmatrix}\varphi\rho_g u_g A\\(1-\varphi)\rho_p u_p A\\\varphi\rho_g u_g^2 A\\(1-\varphi)(\rho_p u_p^2+R_p)A\\\varphi\rho_g u_g(e_g+u_g^2/2+p/\rho_g)A\end{pmatrix} \tag{8}$$

While, the components of S are the source term functions:

$$S=\begin{pmatrix}S_1\\S_2\\S_3\\S_4\\S_5\end{pmatrix}=\begin{pmatrix}\dot{m}_c A+\sum\dot{m}_{ign}A\\-\dot{m}_c A\\-f_s A+\dot{m}_c u_p A+\sum\dot{m}_{ign}u_{ign}A-(\varphi A)\nabla p\\f_s A-\dot{m}_c u_p A-(1-\varphi)A\nabla p\\-Q_p A-f_s u_p A+\dot{m}_c A(e_p+p/\rho_p+\\u_p\cdot u_p/2)+\sum\dot{m}_{ign}H_{ign}A-p\frac{\partial(A\varphi)}{\partial t}\end{pmatrix} \tag{9}$$

The nonlinear hyperbolic system of differential equations of the established two-phase reactive flow model, Eq.(6), is solved using MacCormack's technique which is an explicit finite difference method with second order accurate in both space and time via two steps, predictor and corrector [17]. At each step of the time marching solution, a small amount of artificial viscosity is added and a Shuman filter enhancement approach is applied to smooth the fluctuations in the predicted results at each time step [23].

The predictor step based on the right hand side with forward difference is:

$$\bar{U}_i^{t+\Delta t}=U_i^t-\frac{\Delta t}{\Delta x}\left(E_{i+1}^t-E_i^t\right)+\Delta t S_i^t+v_i^t \tag{10}$$

Where, the artificial viscosity term v_i^t is calculated as:

$$v_i^t=\frac{C_x\left|p_{i+1}^t-2p_i^t+p_{i-1}^t\right|}{p_{i+1}^t-2p_i^t+p_{i-1}^t}(U_{i+1}^t-2U_i^t+U_{i-1}^t) \tag{11}$$

Where, C_x is an arbitrary specified parameter with typical value within range (0.01-0.3). And, the corrector step based on the right side with rearward difference and substituting the predicted values of the time derivative $\bar{U}_i^{t+\Delta t}$ at time $t+\Delta t$:

$$U_i^{t+\Delta t} = \frac{1}{2}\begin{bmatrix} U_i^t + \bar{U}_i^{t+\Delta t} \\ -\frac{\Delta t}{\Delta x}\left(\bar{E}_i^{t+\Delta t} - \bar{E}_{i-1}^{t+\Delta t}\right) \\ +\Delta t \bar{S}_i^{t+\Delta t} \end{bmatrix} + \bar{v}_i^{t+\Delta t} \tag{12}$$

Where, $\bar{v}_i^{t+\Delta t}$ is the calculated artificial viscosity using the predicted values as follows:

$$\bar{v}_i^{t+\Delta t} = \frac{C_x \left|\bar{p}_{i+1}^{t+\Delta t} - 2\bar{p}_i^{t+\Delta t} + \bar{p}_{i-1}^{t+\Delta t}\right|}{\bar{p}_{i+1}^{t+\Delta t} - 2\bar{p}_i^{t+\Delta t} + \bar{p}_{i-1}^{t+\Delta t}} I \tag{13}$$

$$I = (\bar{U}_{i+1}^{t+\Delta t} - 2\bar{U}_i^{t+\Delta t} + \bar{U}_{i-1}^{t+\Delta t})$$

The Shuman filter approach for the calculated conserved variables can be written as:

$$U_i^t = \frac{1}{k+1}(U_{i-1}^t + kU_i^t + U_{i+1}^t) \tag{14}$$

Where, the weighting factor, k, has limited values which cannot be too small to prevent results fluctuations. The necessary condition for convergence of the presented numerical scheme in this study is the Courant-Friedrichs-Lewy stability criterion [24]. In this model this condition is chosen to be:

$$\frac{c\Delta t}{\Delta x} \le 1, \qquad c = \max\left(|u_g| + |u_p| + |a|\right) \tag{15}$$

Where, c is the largest velocity in the system and a is the speed of sound.

3.2 Adaptive grid and computational domain

The finite computational domain of the present model is divided to 102 grid points in the chamber region before the projectile starts to move. Then, after the base pressure reaches (30MPa) the projectile starts to move. Therefore, the equation of motion of the projectile is essential for representing the cell extension at the projectile base which can be written as:

$$pA = \varphi_1 m_{pr} \frac{dv_{pr}}{dt} \tag{16}$$

Where, p is pressure at the projectile base, A is the barrel cross-section area, φ_1 is the coefficient of secondary work, m_{pr} is the projectile mass and v_{pr} is the projectile velocity. At the moment that the projectile starts to move the displacement of the projectile in the axial direction can be written as:

$$x_j^{n+1} = x_j^n + v_{pr}\Delta t \tag{17}$$

At that time, the last mesh cell of the computational domain begins to expand. To overcome the problem of dynamic expansion of this cell, a grid adaptation algorithm is applied herein. As the projectile moves, the length of the last mesh cell Δx_2 will also increase as shown in Fig. 2., and the grid will be self-adapted according these two conditions:

If $\Delta x_2 \le 1.5\Delta x$, the number of the mesh cells is still constant but the value of Δx_1 is changed to be equal to the value of Δx_2.

If $\Delta x_2 > 1.5\Delta x$, a new mesh cell will be added and the value of $\Delta x1$ will calculated to be equal to the value of Δx_2 - Δx.

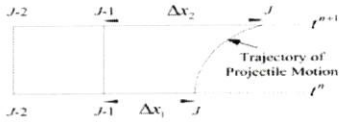

Fig.2 -Schematic of moving control volume.

3.3 Stationary and Moving Boundary Conditions

In this two-phase flow model, a criterion of reflective boundary condition is utilized at the left (breech position) and right (projectile base) boundaries before the shot starts to move. Figure 3 represents two fictitious points at the grid points i= 0 and i=N+1, respectively. These points are required in the calculations at the fixed boundaries and they are located outside the left and right physical domains. The primitive variables of both phases are calculated at the fixed boundary as:

$$\begin{cases} u_0 = -u_1, & u = (u_g, u_p) \\ q_0 = q_1, & q = (\rho_g, p, \varphi, T) \end{cases} \tag{18}$$

Where, u is the velocity vector for both phases and q is a vector representing other primitive variables of the flow.

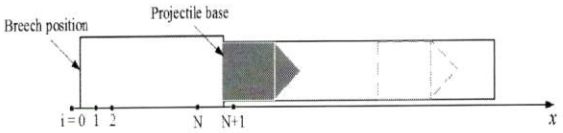

Fig. 3 -Schematic of computational domain.

At the start pressure, the projectile starts to move while the left boundary still stationary. The two-phase flow confined in the chamber behind the projectile starts to move as the chamber pressure and volume is increasing. MCVC method is established to handle the computational domain at the right boundary. Applying the mass conservation on the control volume of the last mesh cell behind the projectile base as shown in Fig.2., the porosity of point j at time t_{n+1} can be calculated via the following procedure :

The solid-phase mass inside the control volume at time t_n and t_{n+1} are calculated as:

$$m_p^n = \left[A\rho_p(1-\varphi)\right]_{j-1/2}^n \left(x_j^n - x_{j-1}^n\right) \tag{19}$$

$$m_p^{n+1} = \left[A\rho_p(1-\varphi)\right]_{j-1/2}^{n+1} \left(x_j^{n+1} - x_{j-1}^{n+1}\right) \tag{20}$$

The mass of solid-phase that flows into the section area A is given by:

$$\Delta m_p = \left[A\rho_p(1-\varphi)u_p\right]_{j-1/2}^{n+1/2} \Delta t \tag{21}$$

The burnet mass of solid-phase from the control volume during time Δt is:

$$\Delta \dot{m}_{br} = -A\dot{m}_c^n (x_j^n - x_{j-1}^n)\Delta t \tag{22}$$

Then, the mass of the solid-phase in the control volume at time $t_{n+\Delta t}$ can be given as:

$$m_p^{n+1} = m_p^n + \Delta m_p + \Delta \dot{m}_{br} \tag{23}$$

In the Eulerian coordinate system, the next relation can be deduced:

$$x_{j-1}^{n+1} = x_{j-1}^n \tag{24}$$

Finally, from Eequations (20) and (24), the porosity can be expressed as:

$$\varphi_{j-1/2}^{n+1} = 1 - \frac{m_p^{n+1}}{A\rho_p (x_j^{n+1} - x_{j-1}^n)} \tag{25}$$

But,

$$\varphi_{j-1/2}^{n+1} = \frac{1}{2}\left(\varphi_{j-1}^{n+1} + \varphi_j^{n+1}\right) \tag{26}$$

Thus, an expression for the porosity of point j at the time $t_{n+\Delta t}$ can be presented as:

$$\varphi_j^{n+1} = 2\varphi_{j-1/2}^{n+1} - \varphi_{j-1}^{n+1} \tag{27}$$

Applying the same previous steps using energy and momentum conservation equations, the remaining primitive flow variables ($u_{g_j}^{n+1}$, $u_{p_j}^{n+1}$, $\rho_{g_j}^{n+1}$ and $e_{g_j}^{n+1}$) can be derived.

4. RESULTS AND DISCUSSIONS

4.1 Numerical verifications

A common test for the accuracy of computational fluid dynamics codes, one dimensional model introduced by G.A. Sod [18], is used to test the ability of MacCormack's algorithm in solving the IBVP for the system of first order, nonlinear coupled partial differential equations with inhomogeneous term possessing shock wave behavior. This test consists of a one dimensional Riemann problem for a tube of unit length $-1 \le x \le 1$. The CFL number is taken to be 0.7 for stability requirements of the solution and the final time is t = 0.2 ms. The initial conditions for the left and right states at t = 0 are:

$$\left.\begin{aligned} \rho(x,0) &= \begin{cases} 1.00 & for \quad x \le 0.0 \\ 0.125 & for \quad x > 0.0 \end{cases} \\ p(x,0) &= \begin{cases} 1.00 & for \quad x \le 0.0 \\ 0.10 & for \quad x > 0.0 \end{cases} \\ u(x,0) &= \begin{cases} 0 & for \quad x \le 0.0 \\ 0 & for \quad x > 0.0 \end{cases} \end{aligned}\right\} \tag{28}$$

Figure 4 shows the computed results of the test compared to the exact solution. It is clear from this figure that there is a good agreement between the numerically calculated results and the exact solution of the Euler system of equations.

4.2 Application of the model to a real large caliber naval guided-projectile gun system

The presented gas-solid flow model in this work is applied to real 130 mm naval gun launching a guided-projectile utilizing granular propellant as described schematically in Fig. 1. The calculated results of some interior ballistic parameters are compared to the experimental data. The input data for the numerical computations which carried out by the code is given in Table 1.

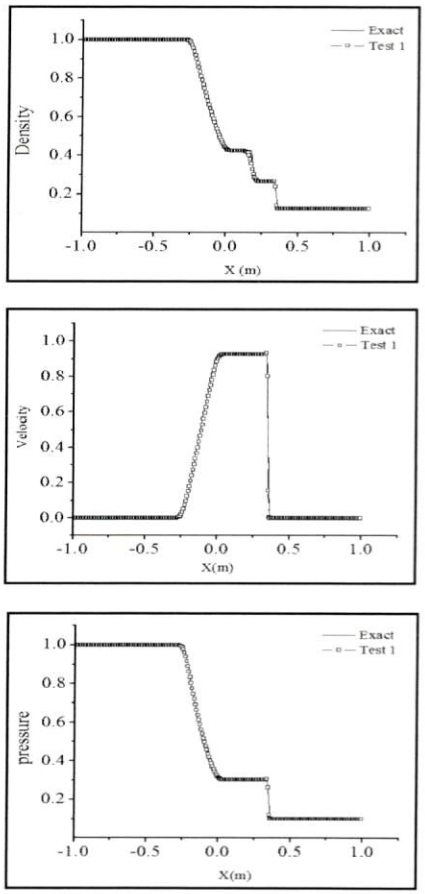

Fig. 4 - Comparison between the numerical and exact solution in 1D Riemann problem.

Table 1 - Input data used in the numerical computations.

Parameter	Value
Geometry:	
Gun caliber (m)	0.130
Barrel length (m)	6.29
Chamber length (m)	0.7
Chamber volume (m3)	0.01366
Projectile mass (Kg)	33.4
Igniter length (m)	0.5
Igniter diameter (m)	0.16
Number of holes of the igniter	60
Hole diameter (m)	0.004
Physical properties:	
Black powder mass (Kg)	0.08
Propellant mass (Kg)	10.6
Propellant co-volume (m3/kg)	0.001
Propellant density (kg/m3)	1600
Propellant force (J/kg)	905000
Propellant ignition temperature (K)	615
Initial porosity	0.56
Start pressure (MPa)	30

4.2.1 Pressure history

Figure 5 shows the calculated pressure history during the interior ballistics process. As the jet of burned gases flow out of the igniter holes into the main propellant charge, the propellant around the vent-holes region starts to burn first and the pressure increases in the gun chamber at about 2.4 ms as shown in Fig. 5a. Due to the pressure gradient, the flame continues to propagate via the unburned regions. At that time a strong shock wave (first shock) occurs towards the direction of projectile base as shown in Fig. 5c-d. By increasing the ignited area, the flame continues to propagate and pressure in the chamber continuously increases. At about 2.9 ms the pressure reaches the start value and the projectile starts to move down the bore. As the projectile moves a rarefaction wave is formed and traveled in the opposite direction towards the gun breech (first rarefaction wave) due to the chamber volume increase following the projectile motion. But, the combustion rate at the breech position is higher than the traveling velocity of the rarefaction wave at that time; therefore a second shock wave is formed and traveled again to the shot base followed by the second rarefaction wave. Similarly, the third shock and rarefaction waves are formed and traveled between the breech and the shot base. As the pressure increases, the projectile velocity increases resulting in attenuation to the pressure wave strength. The chamber pressure reaches its maximum at about 8.4 ms then starts to decrease gradually until the end of the interior ballistics cycle.

4.2.2 Two-phase temperature profile

Figure 6 represents the temperature distribution of the gas phase and propellant particles (solid phase). It is shown from Fig. 6a that the gas temperature is gradually increased in the early stage of combustion compared to the propellant particles that have a more rapid burning rate. At time about 8.6 ms the gas temperature reaches its maximum value. Also it is clear that the temperature distribution near the breech position is higher than that behind the shot base. With the projectile motion the gas temperature is slowly decreases. The ignition wave direction of propagation through the propellant charge bed as well as the wave front is clearly represented in Fig. 6b. The entire propellant charge bed is totally ignited at time about 3.25 ms as it possesses propellant surface temperature of about 615 K.

4.2.3 Two-phase phase velocity profile

The predicted velocity distributions of gas and solid phase during the interior ballistic cycle are shown in Figure 7. It is shown that there are negative velocities in vent-hole region in the early stage of ignition at times about 1.7 ms to 4 ms. The central reason of this negative velocities is the tendency of gas phase combustion products to propagate towards the breech and the projectile base due to pressure gradient inside gun chamber. But, regarding to its high inertia, the solid phase particles are clearly observed to have lower velocity than that of gas phase. This lag of velocity is obvious in the negative velocity region as well as during the whole interior ballistics cycle.

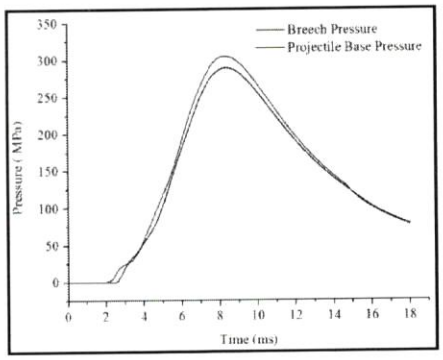

(a) Pressure history versus time.

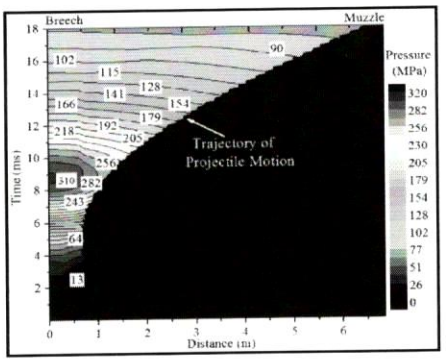

(b) Pressure profile on x-t diagram.

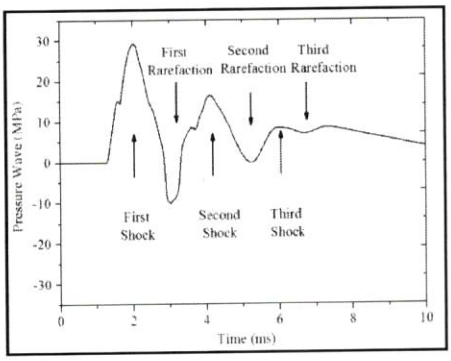

(c) Pressure wave time diagram.

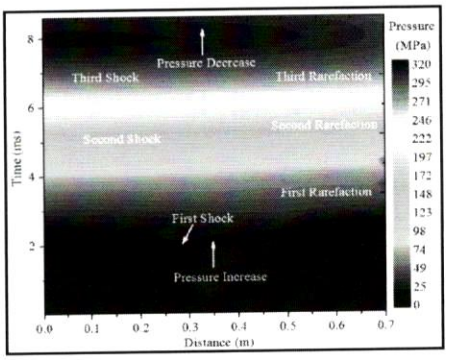

(d) Initial pressure wave distribution.

Fig. 5 - Pressure history during interior ballistic cycle in the 130 mm naval guided-projectile gun system.

4.3 Experimental validation

Due to complication and transient behavior of the interior ballistics process, many parameters can't be measured experimentally except the chamber pressure and the projectile velocity at the muzzle. Table 2 represents the comparison between experimental and computational results for maximum chamber pressure and projectile muzzle velocity. The validation shows a good agreement between experimental and computational results.

Tabale 2 - Comparison between numerical results and experimental results

Ballistic Parameter	Experimental results	Simulation results	Error probability
Maximum chamber pressure (MPa)	319.00	319.45	0.14 %
Muzzle velocity (m/s)	857	861.5	0.52 %

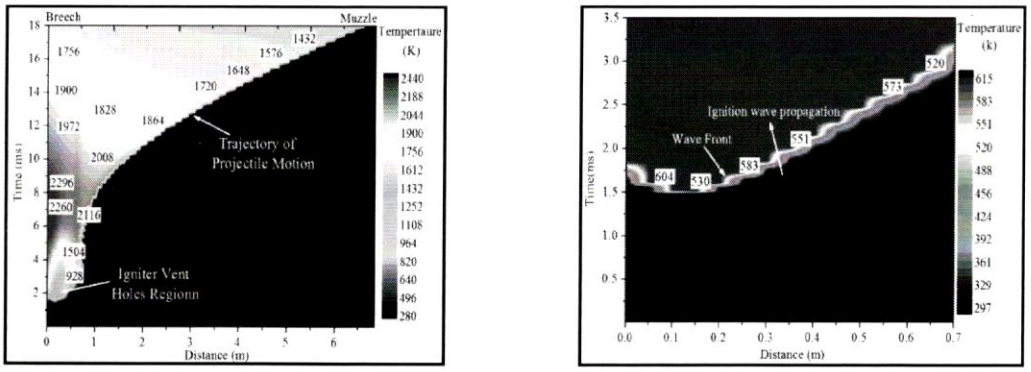

(a) Gas-phase temperature. (b) Solid-phase temperature.

Fig. 6 - Numerical results of the two-phase temperature distribution on x-t diagram.

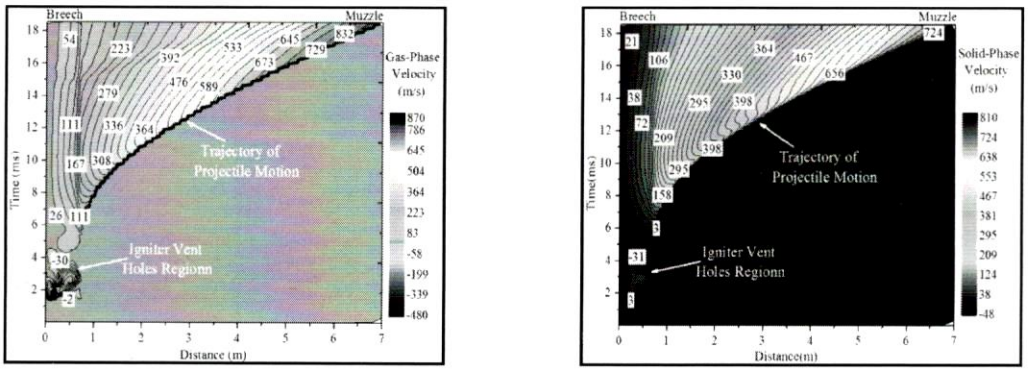

(a) Gas-phase velocity (b) Solid-phase velocity

Fig. 7 - Numerical results of the two-phase velocities on x-t diagram.

5. CONCLUSIONS

In this work, the two-phase flow mathematical model for the solid granular propellant and its products of combustion inside large caliber naval gun guided-projectile system during interior ballistic cycle is described. The ignition of ball propellants in the igniter tube is strongly coupled with the two-phase flow model of the gun chamber. The governing equations are calculated using Maccromack's technique which is an explicit finite difference method with second order accurate in both space and time. The used numerical method is confirmed and validated successfully using Sod shock tube test in order to check its accuracy and aptitude to solve the complex two-phase flow problem. A grid adaptation algorithm is developed and used to deal with the projectile motion with MCVC boundary approach. The interior ballistic performance of a 130 mm NGGPS is closely predicted using this model and a good agreement between experimental and computational results is obtained.

6. REFRENCES

1. M. M.Rashad, X. B. Zhang, and H. Elsadek, Numerical Simulation of Interior Ballistics for Large Caliber Guided Projectile Naval Gun, *J. of Eng. and Appl. Sci*, vol. 60, pp. 201-220., 2013.
2. P. G. Baer, and J. M. Frankle, The Simulation of Interior Ballistic Performance of Guns by Digital Computer Program. BRL, USA ARDC, Ballistic Research Laboratories, Aberdeen Proving Ground, MD, Report No. 1183, 1962.
3. K. D. Fickie and J. A Grosh, Technique for Code Augmentation. US Army Ballistic Research Laboratory, Aberdeen Proving Ground, MD, BRL-MR-3622, 1987.
4. W. R. Fredrick and S. R. Timothy, A Lumped-Parameter Interior Ballistic Computer Code Using the TTCP Model. BRL, USA ARDC, Ballistic Research Laboratories, Aberdeen Proving Ground, MD, Report No. 3710,1988.
5. Jin Zhi Ming, *Interior ballistics in guns*. Publishing Company, of Beijing Institute of Technology, Beijing, 2004.
6. A. W. Horst, E. K. George, and P. S. Gough, New Directions in Multiphase Flow Interior Ballistic Modeling, BRL, USA ARDC, Ballistic Research Laboratories, Aberdeen Proving Ground, MD, Report No. 3102, 1990.
7. A. J. Budka and J. D. Knapton, Pressure Wave Generation in Gun Systems: A Survey. USA Ballistic Research Laboratories, Aberdeen Proving Ground MD, BRL-MR-2567, 1975.
8. A. W. Horst, I. W. May, and E. V. Clarke, The Missing Link between Pressure Waves and Breech Blows, USA ARRADCOM, Ballistic Research Laboratory, Aberdeen Proving Ground, MD, ARBRL-MR-02849, 1978.
9. I. W. May, and A. W. Horst, Charge Design Considerations and Their Effect on Pressure Waves in Guns, USA ARRADCOM, Ballistic Research Laboratory, Aberdeen Proving Ground, MD, ARBRL-TR-02277, 1980.
10. P. S.Gough, and F. J. Zwarts, Modeling Heterogeneous Two-Phase Reacting Flow. *AIAA J.*, vol17, 1, pp. 17–25,1979.
11. M. R. Baer and J. W. Nunziato, A Two-Phase Mixture Theory for the Deflagration-to-Detonation Transition (DDT) in Reactive Granular Materials, *Int. J. Multiphase Flow*, vol. 12, pp. 861–889, 1986.
12. C. R. Woodley, S. Billett, C. Lowe, W.Speares, and E. Toro, The FHIBS Internal Ballistics Code, *22nd International Symposium on Ballistics*, Vancouver, Canada, pp. 322–329, 2005.
13. R. Acharya and K. K. Kuo, Implementation of Approximate Riemann Solver to Two-Phase Flows in Mortar Systems, *ASME J. Appl. Mech.*, vol. 77, pp. 401-410, 2010.
14. C. Cheng, X. b. Zhang, Modeling of Interior Ballistic Gas-Solid Flow Using a Coupled Computational Fluid Dynamics-Discrete Element Method, *J. of Appl. Mech.*, vol.80, 3, pp. 403-425, 2013.
15. P. S. Gough, Initial Development of Core Module of Next Generation Interior Ballistic Model NGEN, U.S. Army Research Laboratory, Aberdeen Proving Ground, MD., ARL-CR-234,1995.
16. P. S. Gough, Formulation of a Next-Generation Interior Ballistic Code. *Proceedings of the 28th JANNAF Combustion Subcommittee Meeting*, San Antonio, pp. 321–337, 1991.
17. M. J. Nusca and P. S. Gough, Numerical Model of Multiphase Flows Applied to Solid Propellant Combustion in Gun Systems,*AIAA joint propulsion conference,* vol. 98, pp. 1-18, 1998.
18. Y. X. Yuan and X. B. Zhang, *Multiphase Hydrokinetic Foundation of High Temperature and High Pressure*, Publishing Company of Harbin Institute of Technology, Harbin, China, 2005.
19. C. J. Ma and X. B. Zhang, Simulation of Contamination Prevention for Optical Window in Laser Ignition Systems of Large-Caliber Guns, *ASME J. Appl. Mech.*, vol. 78, 5, pp. 051014, 2011.
20. J. S. Jang, H.G.Sung, T. S. Roh, and D. W. Choi, Numerical Study on Properties of Interior Ballistics According to Solid Propellant Positions in Chamber, *26th International Symposium on Ballistic*s, Miami, pp. 721–730, 2011.
21. J. D. Anderson, *Computational fluid dynamics: The basics and applications*, McGraw-Hill, New York, 1995.
22. G. A. Sod, A Survey of Several Finite Difference Methods for Systems of Nonlinear Hyperbolic Conservation Laws, *J. of Comput. Phys.*, vol. 27, pp. 1-31, 1978.
23. S. G. Ahmed, A new algorithm for moving boundary problems subject to periodic boundary conditions, *Int. J. of Numer. Meth. for Heat & Fluid Flow*, vol. 16, pp. 18-27, 2006.
24. I. Demirdžić, and M. PerićFinite, volume method for prediction of fluid flow in arbitrarily shaped domains with moving boundaries, *Int. J. Numer. Meth. Fluids*, vol. 10, pp. 771–790, 1990.
25. A. Van Dam and P. A. Zegeling, A Robust Moving Mesh Finite Volume Method Applied to 1D Hyperbolic Conservation Laws from Magnetohydrodynamics, *J. of Comput. Phys.*, vol. 216, pp.526–546, 2006.
26. K. Herman and S. Rajan, Flame Spreading and Combustion in Packed Beds of Propellant Grains, *AIAA*, vol. 75, pp. 1-11, 1975.

27. W. Yu and X. B. Zhang, Aerodynamic Analysis of Projectile in Gun System Firing Process, *ASME J. Appl. Mech.*, , vol. 77, 5, pp. 051406, 2010.
28. C. Lowe, CFD Modeling of Solid Propellant Ignition. Ph.D. thesis, Cranfield University, Cranfield, 1996.
29. K.Alexander, and L.Yu, New Adaptive Artificial Viscosity Method for Hyperbolic Systems of Conservation, Laws. *J. of Comput. Phys.*, vol 231, pp. 8114–8132, 2012.
30. Kawai, S., Lele, S.K.Localized Artificial Viscosity and Diffusivity Scheme for Capturing Discontinuities on Curvilinear and Anisotropic Meshes. Center for Turbulence Research Annual Research Briefs, 2007.
31. E. J. Caramana, M. J. Shashkov, and P. P. Whalen, Formulations of Artificial Viscosity for Multi-dimensional Shock Wave Computations, *J. of Comput. Phys.*, vol. 144, pp. 70–97, 1998.
32. P. N. Stephan, and L. W. Michael, Three Dimensional Shuman filter, *J. of Appl.Meteorology*, vol.19, pp. 464-469, 1980.
33. A. Harten, G. Zwas, Switched Numerical Shuman Filters for Shock Calculations, *J. of Eng. Math.*, vol. 6, 1972.
34. R. Courant, K. O. Friedrichs and Lewy, On the Partial Difference Equations of Mathematical Physics, *IBM J. of Research and Development*, vol. 11, pp. 215–234, 1964.
35. E. F. Toro, *Riemann Solvers and Numerical Methods for Fluid Dynamics: a Practical Introduction*,3rd Edition, Springer Verlag, 2009.
36. Carlo Bartoli, Fast, Transient Heat Transfer Analysis at Gas-solid Interface, Int. J. Of Heat and Technology, vol. 26, pp. 27-32, 2008.
37. F. Askri, M. Ben Salah and S. Ben Nasrallah, Numerical Prediction of Coupled Conduction, Convection and Radiation Heat transfer, Int. J. Of Heat and Technology, vol. 27, pp. 79-86, 2009.